

pubs.acs.org/crystal Communication

Polymorphic Phase Transformation Pathways under Nanoconfinement: Flufenamic Acid

Keke Zhang,[#] Noalle Fellah,[#] Vilmalí López-Mejías, and Michael D. Ward*



Cite This: Cryst. Growth Des. 2020, 20, 7098-7103



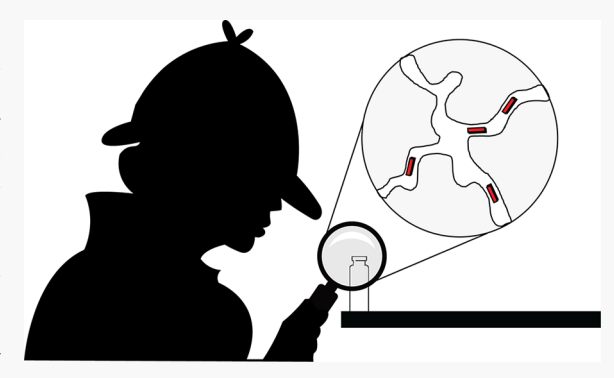
ACCESS

Metrics & More



Supporting Information

ABSTRACT: Flufenamic acid (FFA) is a highly polymorphic compound, with nine forms to date. When melt crystallization was performed under nanoscale confinement in controlled pore glass (CPG), the formation of the extremely unstable FFA form VIII was favored. Under confinement, form VIII was sufficiently stable to allow the measurement of its melting point, which decreased with decreasing pore size in accord with the Gibbs—Thomson relationship, enabling determination of the otherwise elusive melting point of the bulk form. Moreover, the transformation pathways among the various polymorphs depended on pore size, proceeding as form VIII → form II → form I for nanocrystals embedded in 30—50-nm diameter pores, and form VIII → form IV → form III in 100—200 nm pores. In contrast, form VIII converts directly to form III in the bulk. Whereas previous reports have demonstrated that



nanoconfinement can alter (thermodynamic) polymorph stability rankings, these results illustrate that nanoscale confinement can arrest and alter phase transformations kinetics such that otherwise hidden pathways can be observed.

Polymorphism in solid-state materials can be a double-edged sword. The dependence of physicochemical properties on crystal structure can result in new, and possibly advantageous, functions in metastable polymorphs. Conversely, the unanticipated appearance of a new crystal form of a commercial compound can be costly. These characteristics are particularly important in the pharmaceutical sector, for which the efficacy and regulatory compliance of active pharmaceutical ingredients (APIs) often hinge on a particular polymorph. Consequently, the discovery of new forms, the factors influencing their occurrence, and characterization of polymorphic phase transitions are paramount.

A variety of crystallization approaches and conditions for control of polymorphism have been explored, including crystallization in supramolecular gels, ⁸⁻¹⁰ under confinement, ¹¹⁻¹⁵ on heterogeneous templates, ¹⁶⁻²⁰ and from melts. ²¹⁻²³ In many cases, metastable polymorphs have been realized, ^{17,19,22} only to transform rapidly under mild heating or mechanical contact to more stable forms. This behavior can preclude determination of the thermal properties of metastable forms. Crystallization under nanoscale confinement in porous polymer monoliths or controlled pore glass, however, can circumvent these obstacles. ^{11,24} Moreover, the sizes of organic crystals grown under nanoscale confinement are not appreciably different than those expected at or near the size of critical nuclei. ^{11,25} Consequently, nanoconfinement allows the manipulation and examination of crystallization, as well as transformation pathways, at a length scale for which the kinetics of crystallization and thermodynamics of nuclei

intersect.¹¹ This has been most apparent in the observation of size-dependent polymorphism, in which normally metastable phases become thermodynamically favored forms when confined in nanoscale pores.^{26,27} The influence of nanoscale confinement on polymorphic transformation pathways, however, remains under-reported,^{28,29} especially for highly polymorphic systems. While several kinds of nanoporous matrices have been investigated,^{30,31} the refractory character and high loading capacity of controlled pore glass (CPG) permits direct characterization of thermal and phase transitions for compounds presenting polymorphism.

Flufenamic acid (FFA), an API prescribed for the treatment of rheumatoid arthritis, osteoarthritis, and other inflammatory conditions, ³² remains one of the most remarkable and well-studied examples of polymorphism, with nine forms reported. ^{33–44} The first crystal structure (later named form III³³) was reported in 1973, ⁴⁵ followed by the determination of form I nearly 10 years later. ⁴⁶ Forms I and III are enantiotropically related, with form I identified as the metastable form below the transition temperature (42 °C). ³³ The rich polymorphism of FFA has prompted various

Received: August 31, 2020 Revised: October 3, 2020 Published: October 15, 2020





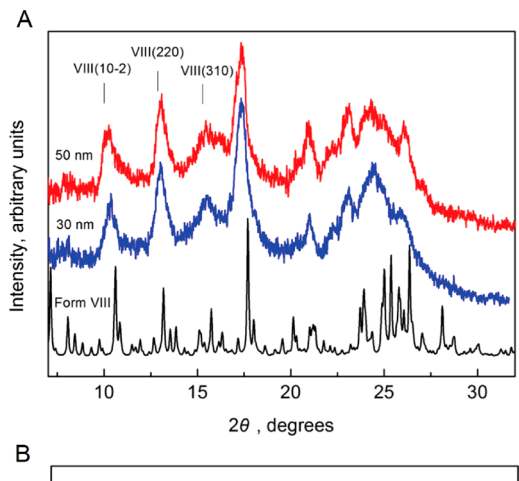
strategies for polymorph control, including the use of soluble additives³⁷ and polymer-induced heteronucleation.¹⁷ The latter approach enabled the discovery of the remaining seven forms, six of which (form II, and forms IV-VIII) formed crystals suitable for single crystal structure determination (Table S1). Form IX was identified as a unique form using powder X-ray diffraction (PXRD). Enthalpy measurements and lattice energy calculations for forms I-VII established form III as the thermodynamically stable form. 17 Rapid transformation of form VIII directly to form III upon heating, mechanical contact, or exposure to ambient humidity precluded the determination of form VIII thermal properties, suggesting that form VIII is the least stable polymorph among those for which single crystal structures have been reported. Herein, we describe the polymorphic behavior of FFA when grown under nanoscopic confinement within CPG. Whereas previous reports have demonstrated that nanoconfinement can alter (thermodynamic) polymorph stability rankings, the results here illustrate that nanoscale confinement can arrest and alter the kinetics of polymorphic phase transformations such that otherwise elusive transformation pathways can be observed. Moreover, the thermal properties of the otherwise fleeting metastable form VIII can be investigated. These observations may have considerable impact on important technology sectors, such as organic electronics and pharmaceuticals, where nanocrystal devices and formulations are becoming increasingly prevalent. 12,47,48

Flufenamic acid (FFA)

Crystal growth of FFA under confinement was performed in a differential scanning calorimeter (DSC) to enable direct measurement of thermal properties and polymorphic phase transformation behavior. Commercially obtained bulk crystals of FFA (form I) were mixed with CPG beads, a borate-silicate composite glass from which the borate phase has been leached to produce a silica glass bead with a random and continuous pore network. The mixture was hermetically sealed in an aluminum DSC pan and heated to 150 °C, above the FFA melting point ($T_{\rm m} = 135$ °C). The pan and its contents were then held at this elevated temperature for 5 min to ensure infiltration of the CPG pores with FFA melt via capillary action. Thermogravimetric analysis indicated negligible weight loss (<1%, Figure S1) at this temperature. The embedded melt was then cooled in the aluminum pan at a controlled rate (10 °C/min) to 25 °C. This resulted in crystallization of FFA nanocrystals embedded within the nanopores, as evident from distinct Bragg peaks in PXRD data. The extent of pore filling has been reported to have minimal effect on the change of melting temperature for a particular pore size. 24,49 The amount of FFA used ensured that ca. 75% of the pores were filled based on the mass ratio of FFA and CPG, using the pore volume specifications supplied by the manufacturer. This also prevented overfilling of the nanopores, which otherwise would result in a thermal signature of the bulk material.

Crystalline FFA was not evident from PXRD or DSC in 4 and 8 nm CPG. The infiltration of FFA was corroborated by the increased mass of the CPG beads, indicating that an

amorphous form was embedded within these ultrasmall pore sizes. The embedded FFA in 4 and 8 nm CPG has remained amorphous for at least six months, when this manuscript was submitted. The stability of the amorphous form can be attributed to either a thermodynamic stability at these small sizes or frustration of nucleation imposed by pore dimensions smaller than the critical size. Notably, solid-state NMR investigations revealed amorphous FFA was stable in silica gels with comparable pore sizes. 40 In contrast, PXRD of FFA embedded in CPG with pore sizes ranging 30-200 nm revealed form VIII with signature peaks at $2\theta = 10.4^{\circ}$, 13.0° , and 15.4° (Figure 1).17 Peak assignments were made based on simulated PXRD patterns calculated from the single crystal structures (REFCODE = FPAMCA).¹⁷ The PXRD data revealed that crystallization was detectable within 30 min for FFA embedded in 100, 140, and 200 nm CPG pores. In contrast, crystallization of FFA embedded in 30 and 50 nm CPG required at least 3 h. Additional PXRD peaks at 2θ =



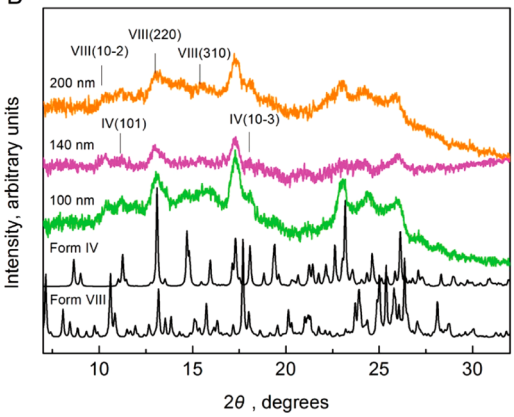


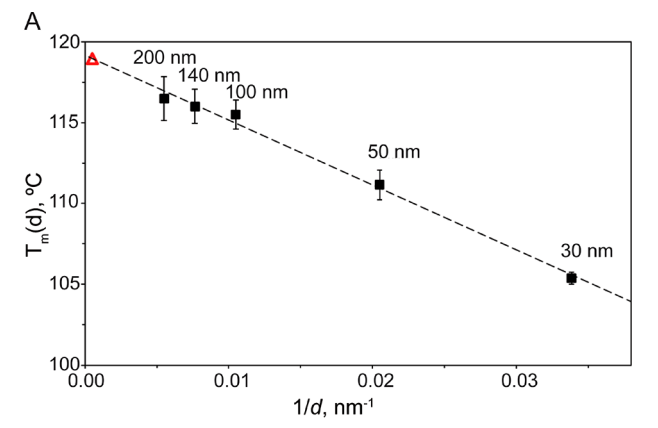
Figure 1. (A) PXRD patterns of FFA embedded in 30 and 50 nm CPG pores measured at room temperature. The black traces correspond to the simulated PXRD patterns of form VIII (REFCODE = FPAMCA13). (B) PXRD patterns of FFA embedded in 100, 140, and 200 nm CPG pores measured at room temperature. The black traces correspond to simulated PXRD patterns of form VIII (REFCODE = FPAMCA13) and form IV (REFCODE = FPAMCA15). Simulated PXRDs were generated from the crystallographic information files (CIF files) obtained from the Cambridge Structural Database. The simulated PXRD pattern of FFA form VIII was obtained from single crystal data collected at 85 K. Consequently, the diffraction peaks for the simulated patterns are shifted slightly to higher 2θ values compared with the experimental patterns acquired at room temperature.

 11.1° and $2\theta = 18.0^{\circ}$, corresponding to form IV, were observed for crystals embedded in 100, 140, and 200 nm pores. The appearance of form IV peaks in Figure 1B was attributed to partial transformation of form VIII to form IV (Figures S2, S3, and S4). PXRD of FFA mixed with nonporous glass beads, used as a control, revealed the crystallization of form IV only (Figure S5).

The crystallization of ice,⁵⁰ metals,⁵¹ and organic solids^{26,49,52,53} in nanoporous matrices has revealed that crystal properties, such as melting points and enthalpies, can be affected dramatically by the size constraints imposed by ultrasmall pores. 54 This behavior is a direct consequence of the competitive balance between surface and volume free energies as crystal size is reduced, and it can be explained by the critical size concept invoked by classical nucleation theory. 11,25,30 As such, the thermotropic signatures under confinement effectively provide a snapshot of crystal properties along the nucleation pathways responsible for polymorph transformations. Previous studies have reported that the melting temperature of form VIII cannot be measured due to the rapid conversion of form VIII to form III upon heating or mechanical contact. The DSC data collected here for embedded FFA in various pore sizes exhibited exothermic peaks at temperatures below 60 °C assignable to the crystallization of the amorphous form, as well as endothermic peaks assignable to the melting of form VIII (Figure S6A). The breadth of the endotherms can be attributed to the variance in the CPG pore sizes $(\pm 10\%)$ as well as pore junctions inherent to CPG. The absence of an endothermic event prior to melting was consistent with exclusive melting of form VIII rather than a phase transition. Overall, these data indicate that confinement arrests the kinetics of the transformation of form VIII to other polymorphs, effectively altering the behavior from enantiotropic to monotropic.

The melting temperature of nanoconfined form VIII, based on triplicate measurements, decreased monotonically from 116.5 °C in 200 nm pores to 105.4 °C in 30 nm pores (Figure 2A). The Gibbs-Thomson equation (eq 1a) predicts a linear relationship between $T_{\rm m}(d)$ and the inverse pore size (1/d), where ΔT_{m} is the melting point depression, $T_{\mathrm{m,bulk}}$ is the bulk melting temperature, $T_m(d)$ is the melting temperature of the confined crystals with a diameter d (assumed to be of equivalent size to the host pore), $\gamma_{crystal-melt}$ is the crystal-melt interfacial energy, $\rho_{\rm solid}$ is the density of crystal, $\Delta H_{\rm fus,bulk}$ is the enthalpy of fusion, d is the pore size, and θ is the contact angle between an idealized spherical nucleus and the interior pore wall. A simplified form that assumes $\theta = 180^{\circ}$ is often used (eq. 1b).^{49,52,55*} The melting points measured for form VIII conform to the linear dependence on 1/d expected for Gibbs-Thomson behavior (Figure 2A). Extrapolation to the ordinate, where 1/d = 0 corresponds to the bulk length scale, affords an onset bulk melting temperature for form VIII of 118.9 \pm 0.4 °C. In the absence of confinement, the instability of form VIII toward transformations to other polymorphs precludes determination of its melting point by conventional means.¹⁷ Notably, the amorphous to crystalline transformation temperatures also increased with decreasing pore size (Figure S6B).

The classical Gibbs–Thomson equation, which predicts a linear dependence of the melting temperature on the inverse of the pore diameter, is predicated on a constant bulk enthalpy $(\Delta H^{\infty}_{\text{fus}})$. The experimental data of the melting point depression of FFA, however, exhibited a linear dependence



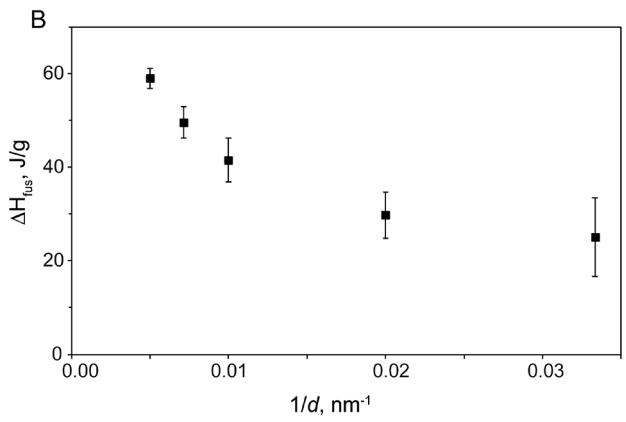


Figure 2. (A) Dependence of the melting temperature, $T_{\rm m}$, on the inverse of the pore diameter, 1/d, for form VIII. The diameters correspond to the nominal CPG pore sizes, as determined by the vendor. The contact angle θ in eq 1a is assumed to be 180°. The dashed line represents the best linear fit to the data set ($R^2 = 0.9931$). $T_{\rm m,bulk}$ of form VIII is denoted as the red open triangle and corresponds to the extrapolated value of 118.9 °C. These experiments were performed in triplicate. The error bars for 30 nm pores are within the size of the square. (B) Dependence of the enthalpy of fusion, $\Delta H_{\rm fus}$, for FFA in CPG beads with nominal pore sizes of 200, 140, 100, 50, and 30 nm.

on 1/d despite the observation that $\Delta H_{\rm fus}$ also decreased with increasing 1/d (Figure 2B). This has been explained $^{26,52,55-57}$ by a compensating reduction in $\gamma_{\rm crystal-melt}$ cos θ or, equivalently recasting the classical Gibbs—Thomson equations in a form wherein $\gamma_{\rm crystal-melt}$ cos θ is replaced by with $\gamma_{\rm crystal-substrate}$ — $\gamma_{\rm melt-substrate}$ using the Young-Dupré equation (eq 1c). The magnitude of $\gamma_{\rm crystal-substrate}$ — $\gamma_{\rm melt-substrate}$ is expected to decrease with decreasing nanocrystal size, thereby offsetting the decreasing $\Delta H_{\rm fus}$ with decreasing pore size, such that the data in Figure 2A retains linearity. Alternatively, this compensating effect may be associated with the formation of a disordered liquid layer between the pore walls and the crystallizing material, which would be expected to become more significant as the pore size is decreased.

$$\Delta T_{\rm m} = T_{\rm m,bulk} - T_{\rm m}(d)$$

$$= -\frac{4T_{\rm m}}{d\Delta H_{\rm fus,bulk} \rho_{\rm solid}} \gamma_{\rm crystal-melt} \cos \theta$$
(1a)

$$\Delta T_{\rm m} = T_{\rm m,bulk} - T_{\rm m}(d) = \frac{4T_{\rm m}}{d\Delta H_{\rm fus,bulk} \rho_{\rm solid}} \gamma_{\rm crystal-melt}$$
(1b)

$$\begin{split} \Delta T_{\rm m} &= T_{\rm m,bulk} - T_{\rm m}(d) \\ &= \frac{4T_{\rm m}}{d\Delta H_{\rm fus,bull} \mathcal{G}_{\rm solid}} (\gamma_{\rm crystal-substrate} - \gamma_{\rm melt-substrate}) \end{split} \tag{1c}$$

Form VIII embedded in 30 nm CPG pores was stable for 3 days under ambient conditions, after which transformation to form II was detected by PXRD (Figure 3A). The transformed

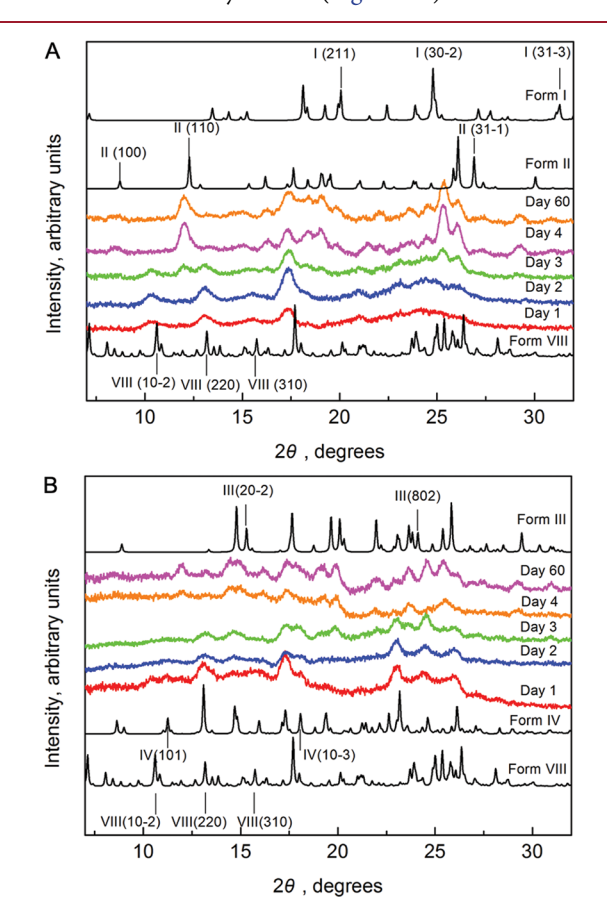


Figure 3. (A) PXRD patterns of FFA embedded in 30 nm CPG pores measured at room temperature. Simulated PXRD patterns of form VIII (REFCODE = FPAMCA13), form II (REFCODE = FPAMCA17), and form I (REFCODE = FPAMCA18) are denoted as black traces. (B) PXRD patterns of FFA embedded in 100 nm CPG measured at room temperature. Simulated PXRD patterns of form VIII (REFCODE = FPAMCA13), form IV (REFCODE = FPAMCA15), and form III (REFCODE = FPAMCA19) are denoted as black traces.

form II was stable in 30 nm pores for more than six months under ambient conditions, after which partial conversion to form I was observed. Form VIII embedded in 50 nm pores began transforming to form II after 3 days. Conversion of form II to form I commenced on the fourth day (Figure S7). The conversion to form I continued slowly over six months, after which some form II remained. These results are consistent with a phase transformation pathway form VIII \rightarrow form II \rightarrow form I in 30 and 50 nm pores. Unlike the behavior observed in 30 and 50 nm CPG, form VIII nanocrystals embedded in 100, 140, and 200 nm CPG began transforming to form IV, rather than form II, within 30 min after cooling to room temperature from the melt (within the time frame of PXRD data collection). By the second day, the form IV nanocrystals

embedded in the larger pores (100, 140, 200 nm) partially transformed to form III (Figures 3B, S8, and S9).

Form VIII crystallized preferentially under nanoconfinement and was kinetically much more stable than in the bulk FFA, which is observed to transform directly to form III when heated, perturbed mechanically, or exposed to ambient humidity. The crystallization of form IV from the melt on the surface of nonporous glass eliminated the possibility that a heterogeneous nucleation mechanism, or the presence of decomposition or impurities, was responsible for the crystallization of form VIII. That is, form VIII is preferred under nanoconfinement because of the size constraints imposed by the pore dimensions in CPGs. According to Ostwald's step rule of stages, 58 intermediate metastable forms crystallize prior to the most thermodynamically stable polymorph. Classical nucleation theory posits that the free energy of a nucleus (and its mature crystal form) is the sum of its surface free energy (positive) and volume free energy (negative).⁵⁹ The nanocrystals embedded in CPG pores are described by a large surface area/volume ratio and, hence, a larger relative contribution from the surface free energy to the total free energy than bulk crystals. Consequently, nanoscale confinement can alter the polymorph stability rankings as well as phase transformation pathways, as the length scale imposed by the CPG pores is comparable to that of crystal nuclei. This is evident from the different pathways associated with the transformation of form VIII when embedded in differently sized pores (Figure 4). Whereas form VIII converts directly to

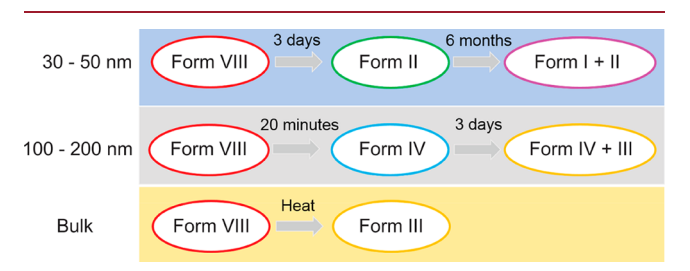


Figure 4. Transition scheme for FFA form **VIII** confined in differently sized nanopores of CPG and in bulk under ambient conditions.

form III in bulk, ¹⁷ form IV emerged as an intermediate between the conversion of form VIII to form III when embedded in pores larger than 50 nm. It is reasonable to suggest that confinement slowed the transformation kinetics of form VIII to form III, which allowed observation of transient form IV. Moreover, form VIII transformed to form I via form II in pores with sizes ≤ 50 nm.

In summary, FFA form VIII, which is extremely unstable and cannot be obtained by conventional solvent-based crystallization methods, was captured from the melt using nanoscale confinement. This permitted determination of the size-dependent melting point for this form as well as an estimate of its bulk melting temperature, which has not been, and likely cannot be, measured directly by any other means. Whereas previous reports have demonstrated that nanoconfinement can alter (thermodynamic) polymorph stability rankings, the results here illustrate that nanoscale confinement can arrest and alter the kinetics of polymorphic phase transformations such that otherwise hidden phase transformation pathways (and their intermediates) can be observed. The dependence of polymorph stability and transformation pathways for nanosized crystals is particularly important for the

pharmaceutical industry where considerable effort has been expended in the development of nanosized APIs by grinding and milling methods for increased bioavailability of poorly water-soluble drugs. The unanticipated transformations of APIs with low aqueous solubility, such as FFA, may pose risks for the certification and efficacy of nanoscale drug formulations. Conversely, control of phase transformations and stabilization of metastable forms through confinement suggests an opportunity for enhanced solubility and delivery of APIs. Although CPG is not a biocompatible matrix, the results suggest that delivery of nanosized metastable crystalline or amorphous APIs confined in appropriate vehicles may be a route for delivering more pharmacokinetically available formulations. G1-63

ASSOCIATED CONTENT

Supporting Information

The Supporting Information is available free of charge at https://pubs.acs.org/doi/10.1021/acs.cgd.0c01207.

Experimental and characterization details and additional figures (PDF)

AUTHOR INFORMATION

Corresponding Author

Michael D. Ward — Department of Chemistry and Molecular Design Institute, New York University, New York City, New York 10003, United States; ⊚ orcid.org/0000-0002-2090-781X; Email: mdw3@nyu.edu

Authors

Keke Zhang — Department of Chemistry and Molecular Design Institute, New York University, New York City, New York 10003, United States; School of Chemical Engineering and Technology, State Key Laboratory of Chemical Engineering, Tianjin University, Tianjin 300072, People's Republic of China

Noalle Fellah — Department of Chemistry and Molecular Design Institute, New York University, New York City, New York 10003, United States

Vilmalí López-Mejías — Department of Chemistry and Crystallization Design Institute, Molecular Sciences Research Center, University of Puerto Rico, San Juan, Puerto Rico 00931, United States; ◎ orcid.org/0000-0003-2138-8414

Complete contact information is available at: https://pubs.acs.org/10.1021/acs.cgd.0c01207

Author Contributions

*K.Z. and N.F. contributed equally to this work.

Notes

The authors declare no competing financial interest.

ACKNOWLEDGMENTS

This work was supported by the National Science Foundation through award number DMR-1708716 and the New York University Materials Research Science and Engineering Center (MRSEC) program of the National Science Foundation under award number DMR-1420073. The X-ray microdiffractometer with GADDS was acquired through the support of the National Science Foundation under Award Number CRIF/CHE-0840277 and NSF MRSEC Program under Award Number DMR-0820341. K. Zhang thanks the support of Prof. Junbo Gong from Tianjin University and the financial support from the China Scholarship Council.

■ REFERENCES

- (1) Di Martino, P.; Guyot-Hermann, A. M.; Conflant, P.; Drache, M.; Guyot, J. C. A new pure paracetamol for direct compression: The orthorhombic form. *Int. J. Pharm.* **1996**, *128*, 1–8.
- (2) Gentili, D.; Gazzano, M.; Melucci, M.; Jones, D.; Cavallini, M. Polymorphism as an additional functionality of materials for technological applications at surfaces and interfaces. *Chem. Soc. Rev.* **2019**, *48*, 2502–2517.
- (3) Chung, H.; Diao, Y. Polymorphism as an emerging design strategy for high performance organic electronics. *J. Mater. Chem. C* **2016**, *4*, 3915–3933.
- (4) Chung, H.; Diao, Y. Polymorphism as an emerging design strategy for high performance organic electronics. *J. Mater. Chem. C* **2016**, *4*, 3915–3933.
- (5) Rietveld, I. B.; Céolin, R. Rotigotine: unexpected polymorphism with predictable overall monotropic behavior. *J. Pharm. Sci.* **2015**, *104*, 4117–4122.
- (6) Elliott, J.; Hancock, B. Pharmaceutical materials science: an active new frontier in materials research. MRS Bull. 2006, 31, 869–873
- (7) Lee, A. Y.; Erdemir, D.; Myerson, A. S. Crystal polymorphism in chemical process development. *Annu. Rev. Chem. Biomol. Eng.* **2011**, 2, 259–280.
- (8) Diao, Y.; Whaley, K. E.; Helgeson, M. E.; Woldeyes, M. A.; Doyle, P. S.; Myerson, A. S.; Hatton, T. A.; Trout, B. L. Gel-induced selective crystallization of polymorphs. *J. Am. Chem. Soc.* **2012**, *134*, 673–684.
- (9) Kaufmann, L.; Kennedy, S. R.; Jones, C. D.; Steed, J. W. Cavity-containing supramolecular gels as a crystallization tool for hydrophobic pharmaceuticals. *Chem. Commun.* **2016**, *52*, 10113–10116.
- (10) Foster, J. A.; Damodaran, K. K.; Maurin, A.; Day, G. M.; Thompson, H. P. G.; Cameron, G. J.; Bernal, J. C.; Steed, J. W. Pharmaceutical polymorph control in a drug-mimetic supramolecular gel. *Chem. Sci.* **2017**, *8*, 78–84.
- (11) Jiang, Q.; Ward, M. D. Crystallization under nanoscale confinement. *Chem. Soc. Rev.* **2014**, 43, 2066–2079.
- (12) Kong, X.; Zong, K.; Lee, S. S. Nanoconfining optoelectronic materials for enhanced performance and stability. *Chem. Mater.* **2019**, 31, 4953–4970.
- (13) Gentili, D.; Manet, I.; Liscio, F.; Barbalinardo, M.; Milita, S.; Bettini, C.; Favaretto, L.; Melucci, M.; Fraleoni-Morgera, A.; Cavallini, M. Control of polymorphism in thiophene derivatives by sublimation-aided nanostructuring. *Chem. Commun.* **2020**, *56*, 1689–1692
- (14) Meldrum, F. C.; O'Shaughnessy, C. Crystallization in confinement. *Adv. Mater.* **2020**, 32, 2001068.
- (15) Anduix-Canto, C.; Kim, Y.-Y.; Wang, Y.-W.; Kulak, A.; Meldrum, F. C.; Christenson, H. K. Effect of nanoscale confinement on the crystallization of potassium ferrocyanide. *Cryst. Growth Des.* **2016**, *16*, 5403–5411.
- (16) López-Mejías, V.; Kampf, J. W.; Matzger, A. J. Polymer-induced heteronucleation of tolfenamic acid: structural investigation of a pentamorph. *J. Am. Chem. Soc.* **2009**, *131*, 4554–4555.
- (17) López-Mejías, V.; Kampf, J. W.; Matzger, A. J. Nonamorphism in Flufenamic Acid and a New Record for a Polymorphic Compound with Solved Structures. *J. Am. Chem. Soc.* **2012**, *134*, 9872–9875.
- (18) Caridi, A.; Kulkarni, S. A.; Di Profio, G.; Curcio, E.; ter Horst, J. H. Template-induced nucleation of isonicotinamide polymorphs. *Cryst. Growth Des.* **2014**, *14*, 1135–1141.
- (19) Roy, S.; Goud, N. R.; Matzger, A. J. Polymorphism in phenobarbital: discovery of a new polymorph and crystal structure of elusive form V. Chem. Commun. 2016, 52, 4389–4392.
- (20) Zhang, K.; Xu, S.; Gong, J.; Tang, W. Revealing the critical role of template functional group ordering in the template-directed crystallization of pyrazinamide. *CrystEngComm* **2019**, *21*, 6382–6389.
- (21) Zhu, Q.; Shtukenberg, A. G.; Carter, D. J.; Yu, T.-Q.; Yang, J.; Chen, M.; Raiteri, P.; Oganov, A. R.; Pokroy, B.; Polishchuk, I.; Bygrave, P. J.; Day, G. M.; Rohl, A. L.; Tuckerman, M. E.; Kahr, B.

- Resorcinol crystallization from the melt: a new ambient phase and new "riddles. J. Am. Chem. Soc. 2016, 138, 4881–4889.
- (22) Shtukenberg, A. G.; Tan, M.; Vogt-Maranto, L.; Chan, E. J.; Xu, W.; Yang, J.; Tuckerman, M. E.; Hu, C. T.; Kahr, B. Melt crystallization for paracetamol polymorphism. *Cryst. Growth Des.* **2019**, *19*, 4070–4080.
- (23) Zhang, K.; Fellah, N.; Shtukenberg, A. G.; Fu, X.; Hu, C.; Ward, M. D. Discovery of new polymorphs of the tuberculosis drug isoniazid. *CrystEngComm* **2020**, 22, 2705–2708.
- (24) Jackson, C. L.; McKenna, G. B. The melting behavior of organic materials confined in porous solids. *J. Chem. Phys.* **1990**, *93*, 9002–9011.
- (25) Davey, R. J.; Schroeder, S. L. M.; ter Horst, J. H. Nucleation of organic crystals—a molecular perspective. *Angew. Chem., Int. Ed.* **2013**, *52*, 2166–2179.
- (26) Ha, J.-M.; Hamilton, B. D.; Hillmyer, M. A.; Ward, M. D. Phase behavior and polymorphism of organic crystals confined within nanoscale chambers. *Cryst. Growth Des.* **2009**, *9*, 4766–4777.
- (27) Fellah, N.; Shtukenberg, A. G.; Chan, E. J.; Vogt-Maranto, L.; Xu, W.; Li, C.; Tuckerman, M. E.; Kahr, B.; Ward, M. D. Disorderly conduct of benzamide IV: crystallographic and computational analysis of high entropy polymorphs of small molecules. *Cryst. Growth Des.* **2020**, *20*, 2670–2682.
- (28) Rengarajan, G. T.; Enke, D.; Steinhart, M.; Beiner, M. Size-dependent growth of polymorphs in nanopores and Ostwald's step rule of stages. *Phys. Chem. Chem. Phys.* **2011**, *13*, 21367–21374.
- (29) Nartowski, K. P.; Malhotra, D.; Hawarden, L. E.; Fábián, L.; Khimyak, Y. Z. Nanocrystallization of rare tolbutamide form V in mesoporous MCM-41 silica. *Mol. Pharmaceutics* **2018**, *15*, 4926–4932.
- (30) Hamilton, B. D.; Ha, J.-M.; Hillmyer, M. A.; Ward, M. D. Manipulating crystal growth and polymorphism by confinement in nanoscale crystallization chambers. *Acc. Chem. Res.* **2012**, *45*, 414–423
- (31) Zhang, S.; Zhang, J.; Zhang, Y.; Deng, Y. Nanoconfined ionic liquids. *Chem. Rev.* **2017**, *117*, *6755*–6833.
- (32) Smyth, C. J.; Bravo, J. F. Antirheumatic drugs: clinical pharmacological and therapeutic aspects. *Drugs* **1975**, *10*, 394–425.
- (33) Kuhnert-Brandstätter, M.; Borka, L.; Friedrich-Sander, G. Zur Polymorphie von Arzneimitteln: Flufenaminsäure und BL 191. *Arch. Pharm.* **1974**, 307, 845–853.
- (34) Krc, J. J. Crystallographic properties of flufenamic acid. *Microscope* 1977, 25, 31–45.
- (35) Galdecki, Z.; Glowka, M. L.; Gorkiewicz, Z. Polymorphism of 2-(3-trifluoromethylphenylamino)benzoic acid. *Acta Polym. Pharm.* **1978**, 35, 77–79.
- (36) Burger, A.; Ramberger, R. Thermodynamische Beziehungen zwischen polymorphen Modifikationen: Flufenaminsäure und Mefenaminsäure. *Microchim. Acta* 1980, 73, 17–28.
- (37) Lee, E. H.; Boerrigter, S. X. M.; Rumondor, A. C. F.; Chamarthy, S. P.; Byrn, S. R. Formation and solid-state characterization of a salt-induced metastable polymorph of flufenamic acid. *Cryst. Growth Des.* **2008**, *8*, 91–97.
- (38) Surov, A. O.; Terekhova, I. V.; Bauer-Brandl, A.; Perlovich, G. L. Thermodynamic and structural aspects of some fenamate molecular crystals. *Cryst. Growth Des.* **2009**, *9*, 3265–3272.
- (39) Hernández Espinell, J. R.; López-Mejías, V.; Stelzer, T. Revealing polymorphic phase transformations in polymer-based hot melt extrusion processes. *Cryst. Growth Des.* **2018**, *18*, 1995–2002.
- (40) Nartowski, K. P.; Malhotra, D.; Hawarden, L. E.; Sibik, J.; Iuga, D.; Zeitler, J. A.; Fábián, L.; Khimyak, Y. Z. 19F NMR spectroscopy as a highly sensitive method for the direct monitoring of confined crystallization within nanoporous materials. *Angew. Chem.* **2016**, *128*, 9050–9054.
- (41) Case, D. H.; Srirambhatla, V. K.; Guo, R.; Watson, R. E.; Price, L. S.; Polyzois, H.; Cockcroft, J. K.; Florence, A. J.; Tocher, D. A.; Price, S. L. Successful computationally directed templating of metastable pharmaceutical polymorphs. *Cryst. Growth Des.* **2018**, *18*, 5322–5331.

- (42) Cookman, J.; Hamilton, V.; Price, L. S.; Hall, S. R.; Bangert, U. Visualising early-stage liquid phase organic crystal growth via liquid cell electron microscopy. *Nanoscale* **2020**, *12*, 4636–4644.
- (43) Sanabria Ortiz, K.; Hernández Espinell, J. R.; Ortiz Torres, D.; López-Mejías, V.; Stelzer, T. Polymorphism in solid dispersions. *Cryst. Growth Des.* **2020**, 20, 713–722.
- (44) Tyler, A. R.; Ragbirsingh, R.; McMonagle, C. J.; Waddell, P. G.; Heaps, S. E.; Steed, J. W.; Thaw, P.; Hall, M. J.; Probert, M. R. Encapsulated nanodroplet crystallization of organic-soluble small molecules. *Chem.* **2020**, *6*, 1755–1765.
- (45) McConnell, J. F. 3'-Trifluoromethyldiphenylamine-2-carboxylic acid, C14H10F3NO2 flufenamic acid. *Cryst. Struct. Commun.* **1973**, 2, 459–461.
- (46) Krishna Murthy, H.; Bhat, T.; Vijayan, M. Structure of a new crystal form of 2-{[3-(trifluoromethyl) phenyl] amino} benzoic acid (flufenamic acid). *Acta Crystallogr., Sect. B: Struct. Crystallogr. Cryst. Chem.* 1982, 38, 315–317.
- (47) Fontana, F.; Figueiredo, P.; Zhang, P.; Hirvonen, J. T.; Liu, D.; Santos, H. A. Production of pure drug nanocrystals and nano cocrystals by confinement methods. *Adv. Drug Delivery Rev.* **2018**, *131*, 3–21.
- (48) Patel, B. B.; Diao, Y. Multiscale assembly of solution-processed organic electronics: the critical roles of confinement, fluid flow, and interfaces. *Nanotechnology* **2018**, *29*, 044004.
- (49) Jackson, C. L.; McKenna, G. B. Vitrification and crystallization of organic liquids confined to nanoscale pores. *Chem. Mater.* **1996**, *8*, 2128–2137.
- (50) Rault, J.; Neffati, R.; Judeinstein, P. Melting of ice in porous glass: why water and solvents confined in small pores do not crystallize? *Eur. Phys. J. B* **2003**, *36*, 627–637.
- (51) Unruh, K. M.; Huber, T. E.; Huber, C. A. Melting and freezing behavior of indium metal in porous glasses. *Phys. Rev. B: Condens. Matter Mater. Phys.* **1993**, 48, 9021–9027.
- (52) Ha, J.-M.; Hillmyer, M. A.; Ward, M. D. Thermotropic properties of organic nanocrystals embedded in ultrasmall crystallization chambers. *J. Phys. Chem. B* **2005**, *109*, 1392–1399.
- (53) Cheng, S.; McKenna, G. B. Nanoconfinement effects on the glass transition and crystallization behaviors of nifedipine. *Mol. Pharmaceutics* **2019**, *16*, 856–866.
- (54) Alcoutlabi, M.; McKenna, G. B. Effects of confinement on material behaviour at the nanometre size scale. *J. Phys.: Condens. Matter* **2005**, *17*, R461.
- (55) Defay, R.; Bellemans, A.; Prigogine, I. Surface tension and adsorption; Longmans: London, 1966.
- (56) Sonnenberger, N.; Anders, N.; Golitsyn, Y.; Steinhart, M.; Enke, D.; Saalwächter, K.; Beiner, M. Pharmaceutical nanocrystals confined in porous host systems interfacial effects and amorphous interphases. *Chem. Commun.* **2016**, *52*, 4466–4469.
- (57) Sun, J.; Simon, S. L. The melting behavior of aluminum nanoparticles. *Thermochim. Acta* **2007**, *463*, 32–40.
- (58) Ostwald, W. Studies on the formation and change of solid matter. Z. Phys. Chem. 1897, 22, 289–302.
- (59) Oxtoby, D. W. Nucleation of first-order phase transitions. *Acc. Chem. Res.* **1998**, 31, 91–97.
- (60) Williams, H. D.; Trevaskis, N. L.; Charman, S. A.; Shanker, R. M.; Charman, W. N.; Pouton, C. W.; Porter, C. J. H. Strategies to address low drug solubility in discovery and development. *Pharmacol. Rev.* 2013, 65, 315.
- (61) Wang, S. Ordered mesoporous materials for drug delivery. *Microporous Mesoporous Mater.* **2009**, 117, 1–9.
- (62) Qian, K. K.; Bogner, R. H. Application of mesoporous silicon dioxide and silicate in oral amorphous drug delivery systems. *J. Pharm. Sci.* **2012**, *101*, 444–463.
- (63) Suresh, K.; López-Mejías, V.; Roy, S.; Camacho, D. F.; Matzger, A. J. Leveraging Framework Instability: A Journey from Energy Storage to Drug Delivery. *Synlett* **2020**, *31*, 1573–1580.